International Journal of Science and Research (IJSR)
ISSN (Online): 2319-7064
Index Copernicus Value (2013): 6.14 | Impact Factor (2013): 4.438

Formability Limit Diagrams of Cold Deep Drawing Process for Nickel 201 Cylindrical Cups

G. Devendar[1], A. Chennakesava Reddy[2]

[1]Research Scholar, Department of Mechanical Engineering, JNT University, Hyderabad -500 085, India

[2]Professor, Department of Mechanical Engineering, JNT University, Hyderabad-500 085, India

Abstract: ***In this present work, a statistical approach based on Taguchi Techniques and finite element analysis were adopted to determine the formability of cylindrical cup from nickel 201 using cold deep drawing process. The process parameters were punch velocity, coefficient of friction, strain rate and displacement per step. The formability of deep drawn cylindrical cups were also constructed. The results obtained from the finite element software namely D-FORM were validated experimentally. The strain rate by itself has a substantial effect on the effective stress, surface expansion ratio, damage and height of the cylindrical cups drawn. The extending deformation of grain boundary micro-voids towards the tensile direction would contribute more to the total elongation, as the strain rate increases; this should be the most possible reason for the increase of surface expansion ratio with an increase in the strain-rate. The plastic deformation increases with the extended yield strength, consequently the damage decreases.***

Keywords: Nickel 201, cold deep drawing, punch velocity, coefficient of friction, strain rate, cylindrical cups, formability

1. Introduction

Cold deep drawing of metal sheet is used to form cans, boxes, and bottles, as well as irregularly shaped products at room temperature. A flat blank sheet is formed into a cup by forcing a punch against the center portion of a blank that rests on the die. The cold deep drawing process variables, which affect the failure of the cup drawing process, include material properties, die design, and process parameters such as coefficient of friction, strain rate, blank holding force, punch velocity, punch and die corner radii and drawing ratio [1, 2].

Experimental [3] and numerical [4-8] investigation of cup drawing was carried out to study of stresses and strains cold and warm drawing environments. In the finite element simulations, a forming limit diagram (FLD) has been successfully applied to analyze the fracture phenomena by comparing the strain status [9-17]. Optimization of the process parameters such as strain rate, blank holder force, friction coefficient, etc., was accomplished based on their degree of importance on the sheet metal forming characteristics. In fact, the metallic material is subjected to large irreversible deformation in sheet forming processes. This leads to high strain localization zones and then internal or superficial micro-defects (ductile damage) This damage causes quality problems such as necking and fracture, leading to process interruptions [18].

Nickel 201 alloy is a nickel-manganese alloy. The manganese addition provides resistance to sulfur compounds at elevated temperatures and retains higher strength than Nickel 200 alloy at elevated temperatures. Nickel 201 alloy has been used as fuses in light bulbs and grids in vacuum tubes.

In the present work, the formability of cold deep drawing process was evaluated during the fabrication of Nickel 201 cylindrical cups. The investigation was focused on the process parameters such as punch velocity, coefficient of friction, displacement per step and strain rate. The design of experiments was carried out using Taguchi technique and the warm deep drawing process was executed using the finite element analysis software namely D-FORM 3D.

2. Materials and Methods

Nickel 201 was used to fabricate cylindrical cups. The levels chosen for the control parameters were in the operational range of Nickel 201 using deep drawing process. The chosen control parameters are summarized in table 1. The orthogonal array (OA), L9 was selected for the present work. The assignment of parameters along with the OA matrix is given in table 2.

Table 1: Control parameters and levels

Factor	Symbol	Level–1	Level–2	Level–3
Punch velocity, mm/s	A	2	3.5	5
Coefficient of friction	B	0.1	0.15	0.2
Strain rate. 1/s	C	1	10	100
Displacement per step	D	0.50	0.75	1.00

Table 2: Orthogonal array (L9) and control parameters

Treat No.	A	B	C	D
1	1	1	1	1
2	1	2	2	2
3	1	3	3	3
4	2	1	2	3
5	2	2	3	1
6	2	3	1	2
7	3	1	3	2
8	3	2	1	3
9	3	3	2	1

2.1 Fabrication of Deep Drawn Cups

The blank size was calculated by equating the surface area of the finished drawn cup with the area of the blank. The diameter meter of the blank is given by:

$D = \sqrt{d^2 + 4dh}$ for $d/r > 20$ (1)

$D = \sqrt{d^2 + 4dh}$ - 0.5r for $20 < d/r < 20$ (2)

$D = \sqrt{d^2 + 4dh}$ - r for $15 < d/r < 10$ (3)

$D = \sqrt{(d - 2r)^2 + 4d(h - r) + 2\pi r(d - 0.7r)}$
for $2d/r < 10$ (4)
where d is the mean diameter of the cup (mm), h is the cup height (mm) and r is the corner radius of the die (mm).

The force required for drawing depends upon the yield strength of the material σ_y, diameter and thickness of the cup:
Drawing force, $F_d = \pi dt\lceil D/d - 0.6\rceil\sigma_y$ (5)
where D is the diameter of the blank before operation (mm), d is the diameter of the cup after drawing (mm), t is the thickness of the cup (mm) and σ_y is the yield strength of the cup material (N/mm^2).

The drawing punches must have corner radius exceeding three times the blank thickness (t). However, the punch radius should not exceed one-fourth the cup diameter (d).
3t<Punch radius < d/4 (6)

For smooth material flow the die edge should have generous radius preferably four to six times the blank thickness but never less than three times the sheet thickness because lesser radius would hinder material flow while excess radius the pressure area between the blank and the blank holder, and would cease to be under blank pressure. The corner radius of the die can be calculated from the following equation:
$r = 0.8\sqrt{(D - d)t}$ (7)

The drawing ratio is roughly calculated as
DR = D/d (8)

The material flow in drawing may render some flange thickening and thinning of walls of the cup inevitable. The space for drawing is kept bigger than the sheet thickness. This space is called die clearance.
Clearance, $c = t + \mu\sqrt{10t}$ (9)

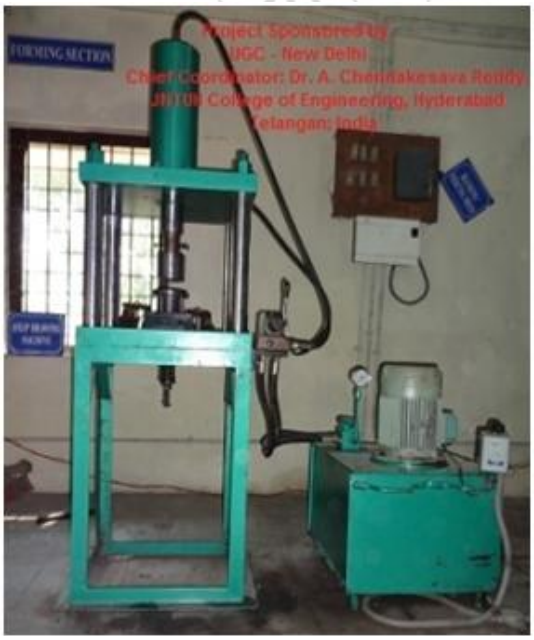

Figure 1: Deep drawing machine (hydraulic type)

The sheets of Nickel 201 were cut to the required blank size. The blank pressure was calculated, as in (5). The cups were fabricated using hydraulically operated deep drawing machine as shown in figure 1.

2.2 Finite Element Modeling and Analysis

The finite element modeling and analysis was carried using D-FORM 3D software. The pyramidal top punch, pyramidal bottom hollow die were also modeled with appropriate inner and outer radius and corner radius using CAD tools. The clearance between the punch and die was calculated as in Eq. (9). The sheet blank was meshed with tetrahedral elements as shown in figure 2. The modeling parameters of deep drawing process were as follows:
Number of tetrahedron elements for the blank: 21980
Number of nodes for the blank: 7460
Number of polygons for top die: 9120
Number of polygons for bottom die: 9600

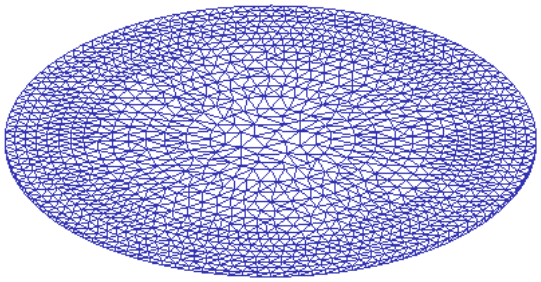
Figure 2: Deep drawing process for pyramidal cups.

The basic equations of the rigid-plastic finite element analysis are as follows:
Equilibrium equation:
$$\sigma_{ij,j} = 0 \quad (10)$$
Compatibility and incompressibility equations:
Strain rate tensor, $\dot{\varepsilon}_{ij} = \frac{1}{2}\left(u_{i,j} + u_{j,i}\right)$, $\dot{\varepsilon}_{kk} = 0$ (11)
where $u_{i,j}$ and $u_{j,i}$ are velocity vectors.
Constitutive equations:
Stress tensor, $\sigma_{ij} = \frac{2\sigma_{eq}}{3\varepsilon_{eq}}\dot{\varepsilon}_{ij}$ (12)
where, equivalent stress, $\sigma_{eq} = \sqrt{\frac{3}{2}\left(\sigma'_{ij}, \sigma'_{ij}\right)}$ and equivalent strain, $\varepsilon_{eq} = \sqrt{\frac{3}{2}\left(\dot{\varepsilon}_{ij}\dot{\varepsilon}_{ij}\right)}$.
The Coulomb's friction model was given by
$$\tau_f = \mu p \quad (13)$$
where μ is the coefficient of friction (COF), p is the normal pressure, and τ_f is the frictional shear stress.
The flow stress based on the strain hardening is computed by the following equation:
$$\sigma_f = K\varepsilon^n \quad (14)$$
where, K and n are work hardening parameters depending on mechanical properties of material.
The flow stress equation considering the effects of the strain, strain rate and temperature is given by
$$\sigma_f = f\left(\varepsilon, \dot{\varepsilon}, T\right) \quad (15)$$
where, ε represents the strain, $\dot{\varepsilon}$ represents the strain rate and T represents the temperature.

Johnson-Cook Model [19] is among the most widely used mode. It connects all the deformation parameters in the following compact form.

$$\sigma_f = [\sigma + K\varepsilon^n]\left[1 + Sln\frac{\dot{\varepsilon}}{\dot{\varepsilon}_0}\right]\left[1 - \left(\frac{T-T_0}{T_m-T_0}\right)^m\right] \quad (16)$$

where, $\dot{\varepsilon}_0$ is a reference strain rate taken for normalization; σ is the yield stress and *K* is the strain hardening factor, whereas *S* is a dimensionless strain rate hardening coefficient. Parameters *n* and *m* are the power exponents of the effective strain and strain rate.

Hill's and Swift's theories used to calculate the forming limit strains on the left and the right side, respectively, of the forming limit diagram (FLD). Assuming that the strain-stress relationship of sheets can be expressed by Hollomon's equation the formulae calculating the forming limit strains can be written as follows, with stress ratio, $\alpha = \sigma_1/\sigma_2$.
For $\varepsilon_2 < 0$

$$\varepsilon_{l1} = \frac{1+(1-\alpha)r}{1+\alpha}n \quad (17)$$

$$\varepsilon_{l2} = \frac{\alpha+(1-\alpha)r}{1+\alpha}n \quad (18)$$

In the present work, the contact between blank/punch and die/blank were coupled as contact pair. The mechanical interaction between the contact surfaces was assumed to be frictional contact and modeled as Coulomb's friction model as defined in Eq. (13). The finite element analysis was chosen to find the effective stress, height of the cup, and damage of the cup. The finite element analysis was carried out using D-FORM 3D software according to the design of experiments.

4. Results and Discussion

Two trials were carried out with different meshes for each experiment. For the ANOVA (analysis of variance) the Fisher's test (F = 3.01) was carried out on all the parameters (A, B, C and D) at 90% confidence level.

4.1 Influence of process parameters on effective stress

Table 3 gives the ANOVA (analysis of variation) summary of the effective stress. The punch velocity (A) had an effect (25.64%) on the effective stress. The coefficient of friction had contributed a variation of 7.54% in the effective stress. The strain rate had a marked effect of 53.74% of the total variation observed in the effective stress. The displacement per step had tendered a variation of 13.08% in the effective stress.

Table 3: ANOVA summary of the effective stress

Source	Sum 1	Sum 2	Sum 3	*SS*	*v*	*V*	*F*	*P*
A	2363	4733	5824	2.1E+06	1	2.1E+06	3.2E+08	25.64
B	3800	5414	3706	6.1E+05	1	6.1E+05	9.4E+07	7.54
C	6950	1835	4134	4.4E+06	1	4.4E+06	6.7E+08	53.74
D	5037	5036	2847	1.1E+06	1	1.1E+06	1.6E+08	13.08
e				6.5E-03	4	0.0E+00	0.0E+00	0.00
T	18150	17017	16511	8.1E+06	8			100.00

Note: *SS* is the sum of square, *v* is the degrees of freedom, *V* is the variance, *F* is the Fisher's ratio, *P* is the percentage of contribution and *T* is the sum squares due to total variation.

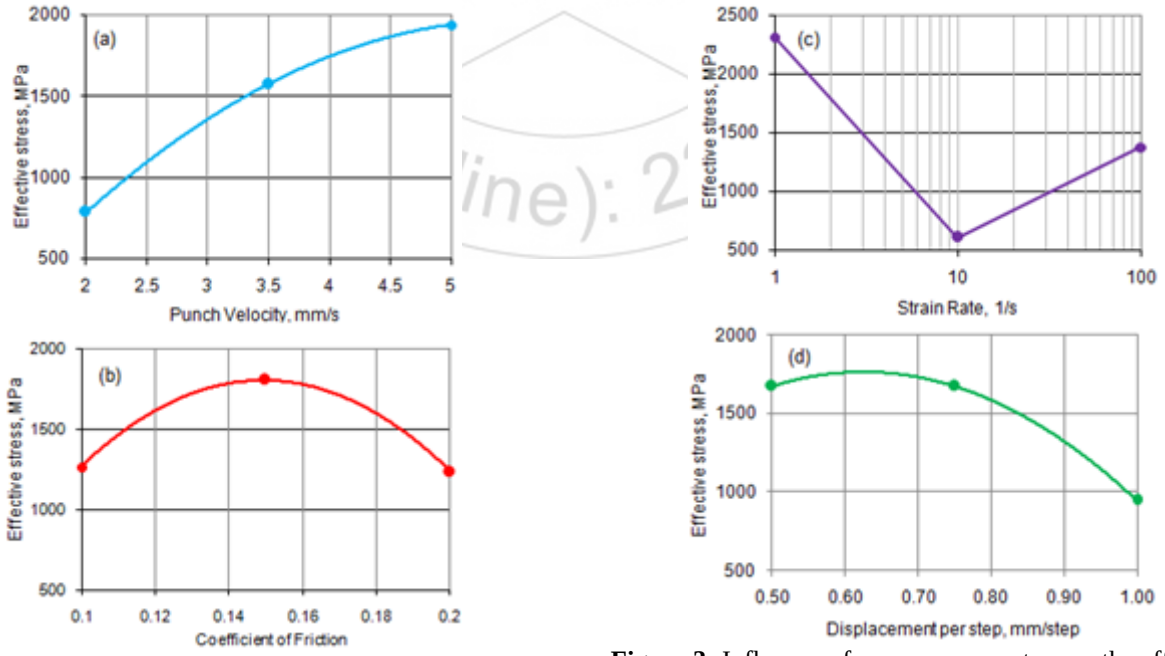

Figure 3: Influence of process parameters on the effective stress: (a) punch velocity, (b) coefficient of friction, (c) strain rate and (d) displacement per step on the effective stress.

The effective stress was increased with an increase in the punch velocity (figure 3a). A material that undergoes higher punch velocity experiences higher punch forces. The use of a high punch velocity can lead to rupture of the sheet material. This phenomenon was also observed in strip drawing tests done by Carignan et al. [19]. The influence of friction on the effective stress is shown in figure 3b. In this work, the coefficient of friction was varied from 0.1 to 0.2. Therefore, the shear stress due to friction would vary from 0.1P to 0.2P, where P is the normal pressure according the Eq. (13). The increase in the nominal contact pressure would crush the surface asperities of the blank giving rise to more real contact area. Hence, the result was the requirement of high drawing pressure to draw the cup. The equivalent stress was high for the coefficient of friction of 0.15. When work hardening occurs, the real pressure in an asperity is larger than the hardness, causing a lower real contact area resulting the low value of effective for coefficient of friction of 0.2. Also, in the drawing process the friction coefficient decreases with increasing drawing velocity. It is known that in warm and hot forming the forming speed and with it combined strain rate has immense role on material flow in bulk and sheet metal operations. In contrast, the influence of the strain rate on the flow curve is only rarely analyzed at room temperature. The required stress in tension necessary to obtain particular deformation is getting higher with increase of a strain rate at a constant temperature. The equivalent stress was increased from 10–100 s^{-1} (figure 3c) while at quasi-static strain conditions below strain rate of 10 s^{-1} the total elongation is smaller and the material rupture at lower equivalent strains. The effective stress decreases with an increase in the displacement per step as shown in figure 3d. In figure 4 the punch force evolution acquired during the numerical deep drawing process was described. Figure 4 presents the punch force evolution with the punch displacement, considering anisotropic and isotropic behaviour of the blank, respectively. Some oscillations in the predicted punch force evolution due to the relation between the blank discretization and the isotropic behavior of the material. Globally, there is always a surface layer of nodes entering or leaving contact with the tools, leading to a globally smoother evolution, presenting more oscillations.

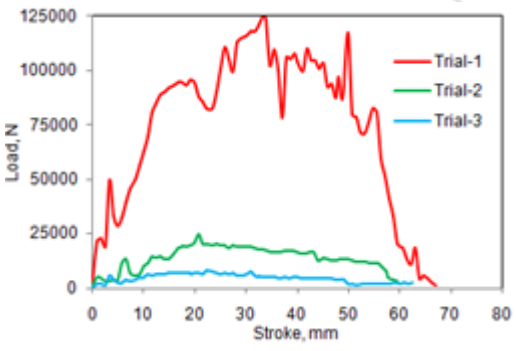

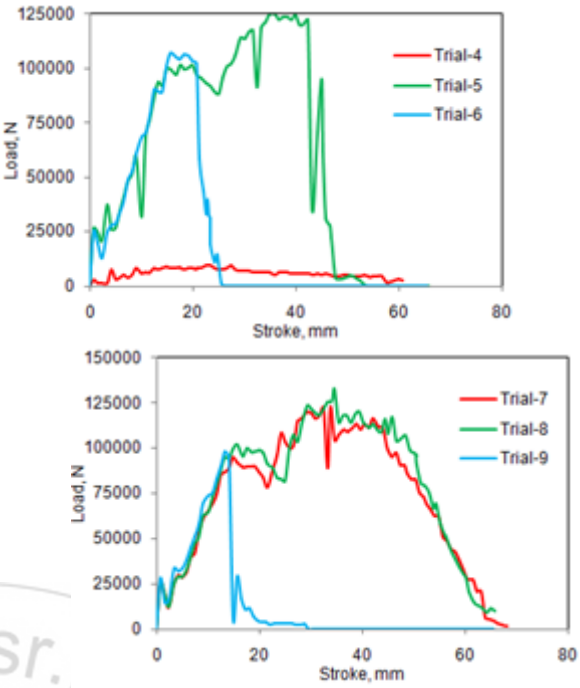

Figure 4: Punch force evolution with the punch displacement

4.2 Influence of Process Parameters on Surface Expansion Ratio

In the deep drawing process the plastic deformation in the surface is much more pronounced than in the thickness. The term surface expansion ratio was introduced to measure the formability of cups [12-17]. This depicts the formability and ductility of the blank material drawn into the cup.

$$\text{Surface expansion ratio} = \frac{A_i}{A_0} \quad (19)$$

where, A_i is the instantaneous surface area of the cup drawn and A_0 is the initial blank surface area.

Table 4: ANOVA summary of the surface expansion ratio

Source	Sum 1	Sum 2	Sum 3	*SS*	*v*	*V*	*F*	*P*
A	6.07	6.38	4.67	0.55	1	0.55	19.93	30.72
B	5.66	5.47	5.99	0.04	1	0.04	1.45	1.71
C	4.71	6.35	6.06	0.5	1	0.5	18.12	27.88
D	4.97	5.32	6.83	0.64	1	0.64	23.19	35.84
e				0.0276	4	0.01	0.36	3.85
T	21.41	23.52	23.55	1.7576	8			100

The ANOVA summary of surface expansion ratio is given in table 4. The punch velocity (A) would contribute 30.72% towards the variation observed in the surface expansion ratio. The coefficient of friction was insignificant the surface expansion ratio. The strain rate and displacement per step, respectively had contributed 27.88% and 35.84% towards the total variation in the surface expansion ratio.

The surface expansion ratio would decrease with an increase in the punch velocity (figure 5a). In the forming processes, the volume of the material remains constant before and after the forming process. The punch force is directly proportional to the punch velocity. On account of the punch force, the blank material undergoes plastic deformation to form the

cup. As the plastic deformation is irreversible, the cup retains its shape. Experimentally, it has been observed that the surface area of the cup drawn is always higher than the initial blank surface area [6]. The coefficient of friction was insignificant on the surface expansion ratio. The effect of strain rate on the surface expansion ratio is shown in figure 5b. The surface expansion ration increased with the strain rate (figure 5b) displacement per step (figure 5c). A sudden change of strain rate from e_1 to e_2 would lead to a corresponding increase of stress from σ_1 to σ_2. After each sudden change of strain rate a stress transient was observed. Depending on the previous deformation history, the stress may be at first either higher or lower than the expected value. The extending deformation of grain boundary micro-voids towards the tensile direction would contribute more to the total elongation, as the strain rate increases; this should be the most possible reason for the increase of surface expansion ratio with an increase in the strain-rate. The FEA results of surface expansion ratio are revealed in figure 6 for various test conditions as per the design of experiments. For the test trails 3 and 4 the surface expansion ratio was higher than 2.5. For the trail 2 the surface expansion ratio was higher than 2.0 but less than that of trials 3 and 4. For the trails 1, 5 to 9 the surface expansion ratio was less than 2.0.

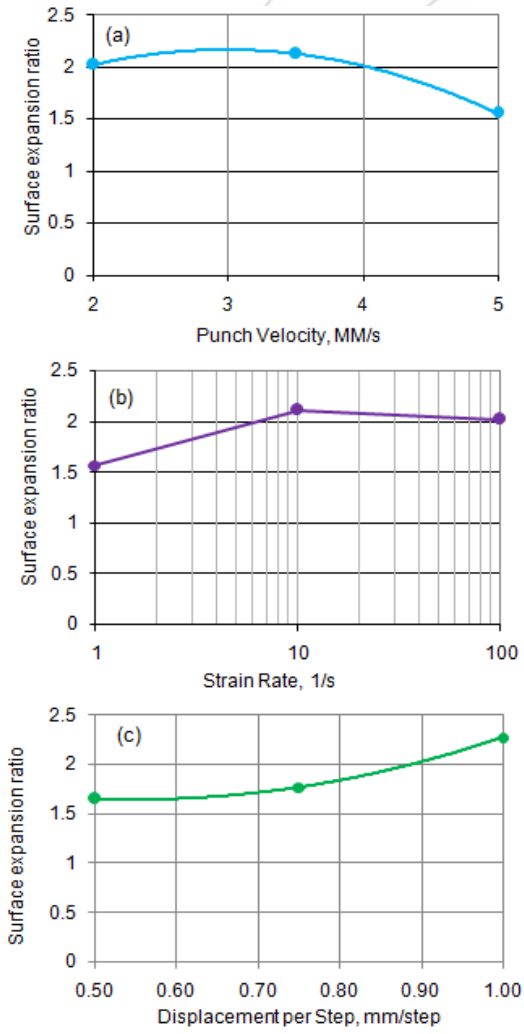

Figure 5: Influence of process parameters on the surface expansion ratio: (a) punch velocity, (b) coefficient of friction, (c) strain rate and (d) displacement per step on the effective stress.

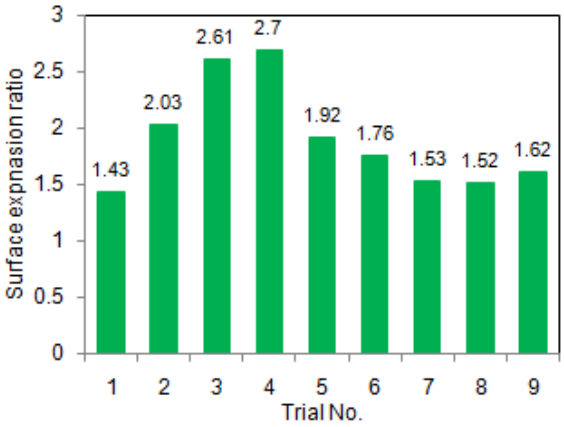

Figure 6: Surface expansion ratios of all trials

4.3 Influence of process parameters on cup height

As per the Fisher's test (F = 3.01), the punch velocity (A) would contribute 14.16% towards the variation observed in the cup heights (table 5). The coefficient of friction gave 56.26% towards the variation in the cup heights. The strain rate would furnish 12.70% towards the variation in the cup heights. The displacement per step would share 16.88% towards the variation in the cup heights.

Table 5: ANOVA summary of the cup height

Source	Sum 1	Sum 2	Sum 3	*SS*	*v*	*V*	*F*	*P*
A	190.20	143.38	150.55	423.95	1	423.95	61598.25	14.16
B	198.64	181.29	104.20	1684.69	1	1684.69	244778.76	56.26
C	158.47	139.07	186.59	380.44	1	380.44	55276.42	12.70
D	138.77	153.33	192.04	505.45	1	505.45	73439.88	16.88
e				0.01	4	0.00	0.00	0.00
T	686.08	617.07	633.38	2994.52	8			100.00

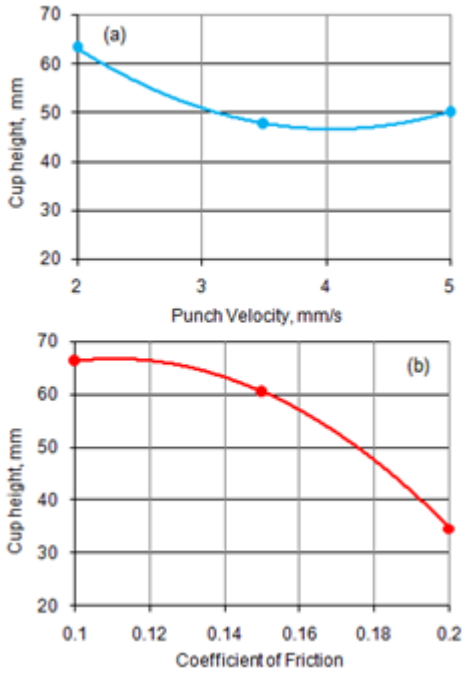

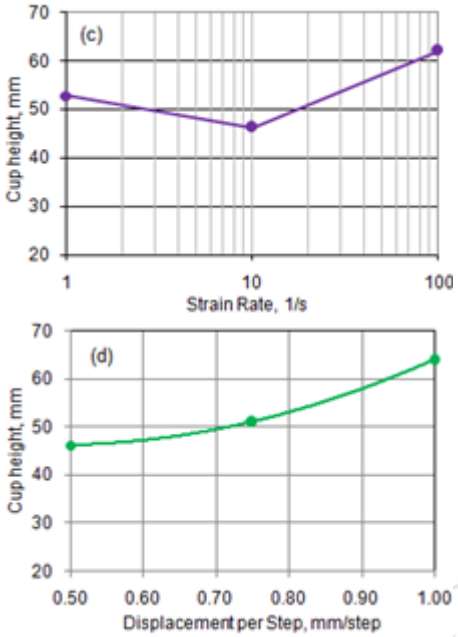

Figure 11: Influence of blank thickness (a) and strain rate (b) on the height of cup

The cup height would decrease with an increase in the punch velocity (figure 11a). The coefficient of friction decreases with increasing of punch velocity. Due to severe friction there may be thinning or failure of the side wall in drawn cup at the flange area. The cup height would increase with an increase in the coefficient of friction as shown in figure 11b. The major influential characteristic of the material is the ductility which depends upon the strain rate. For the strain rate $100s^{-1}$, the cup height was highest. At higher rates of strain the flow stress of material increases leading to higher loads on the equipment. At low strain rates the flow stress increases with increase in strain rate. At higher strain rates it still increases but at a slower rate. For the trials 1, 7 and 8, the cup heights are 67.32 mm, 68.33 mm and 66.07 mm respectively. The lowest cup heights were 25.08 mm and 16.15 mm for trials 6 and 9 respectively. the cup height increases with increase of displacement per step as shown in figure 11d.

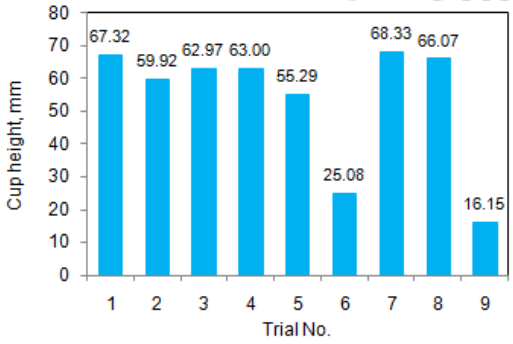

Figure 12: Cup heights under different trials

4.4 Influence of process parameters on damage of cup

The ANOVA summary of damage of cups is given in table 6. When the Fisher's test (3.01) was applied to ascertain the influence of process parameters it was found that the punch velocity (A), and the strain rate (C), respectively had contributed 19.26% and 71.70% of the variation in the damages of cups drawn. The coefficient of friction and displace per step were insignificant on the damages of cups.

Table 6: ANOVA summary of damage of the cups

Source	Sum 1	Sum 2	Sum 3	*SS*	*v*	*V*	*F*	*P*
A	12.40	51.90	73.25	635.51	1	635.51	4.29	19.26
B	25.61	61.58	50.36	225.86	1	225.86	1.52	7.53
C	115.56	3.61	18.37	2466.06	1	2466.06	16.65	71.70
D	20.97	60.16	56.42	311.93	1	311.93	2.11	10.00
e				148.16	4	37.04	0.25	8.49
T	174.53	177.26	198.40	3491.20	8			100.00

The damage factor in the cups is defined as follows:

$$D_f = \int \frac{\sigma_1}{\sigma_{es}} d\varepsilon \qquad (20)$$

where, σ_1 is the tensile maximum principal stress; σ_{es} is the effective stress; and $d\varepsilon$ is the effective strain increment. The damage was increased with punch velocity (figure 13a). However, the damages in the cups was decreased with increase of strain rate as shown in figure 13b. The plastic deformation increases with the extended yield strength, consequently the damage decreases. Precipitation strengthening and solution hardening have raised the yield line. Figure 14 illustrates the damages occurred in the cups drawn under various trials. For the cups drawn with trial conditions of 6 and 8 the damages were recorded to be 46.81 and 56.42 respectively. No damage was noticed in the cups drawn with trial conditions of 3 and 4.

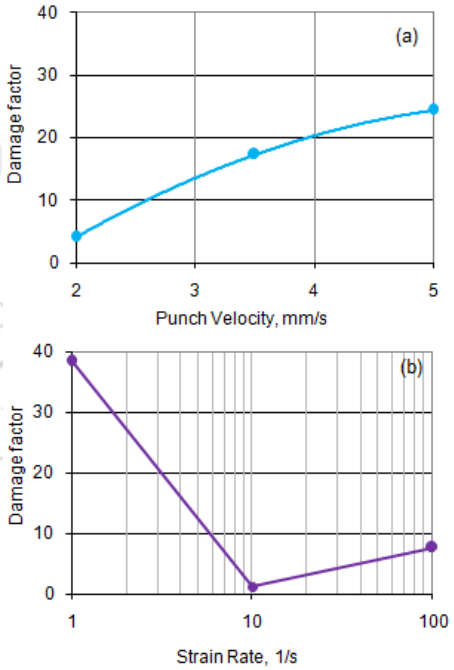

Figure 13: Influence of blank thickness on the damage of cup

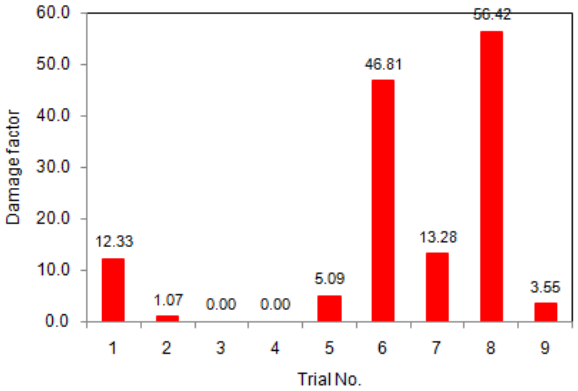

Figure 14: Cup damages under different trials.

Figure 15 depicts the forming limit diagram with damages in the cylindrical cups drawn from nickel 201 sheets of 1.0 mm. The cylindrical cups drawn under trials 1 and 2 were fractured on account of biaxial tension and compression induced in the blank material. The cup 1 was fractured in the flange area while the cup was damaged in the area of punch corner radius. No damage was observed in the cup 3 except wrinkles. The cylindrical cups drawn under trials 4, 5 & 6 were fractured due to uniaxial tension and stretching. No damage occurred in the cup 4. For the cups 5 and , the fracture was observed at the punch corner radius. The cylindrical cups drawn under trials 7 and 8 were torn in the flange area owing to equal biaxial tension, whereas the cups drawn under trial 9 were fractured due to compression at die corner radius (figure 17). The shear strength induced in the cups 3 and 4 was lesser than the shear strength (359 MPa) of nickel 201. For the cups 1, 5, 6, 7, 8, and 9 the shear strength was higher than 359 MPa. Even though the shear strength for the cup 2 was 259 MPa, the cup was damaged at the punch corner radius due to biaxial tension. The deep drawing conditions of trials 3, 4 and 9 are illustrated in figure 19.

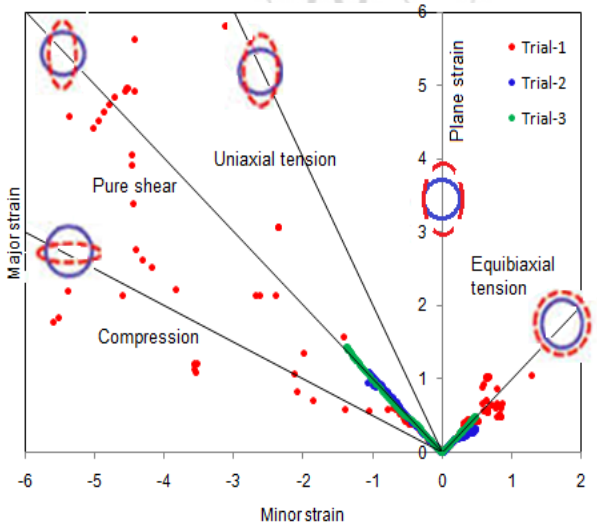

Figure 15: Forming limit diagram with damage in the cups of 0.8 mm blank thickness

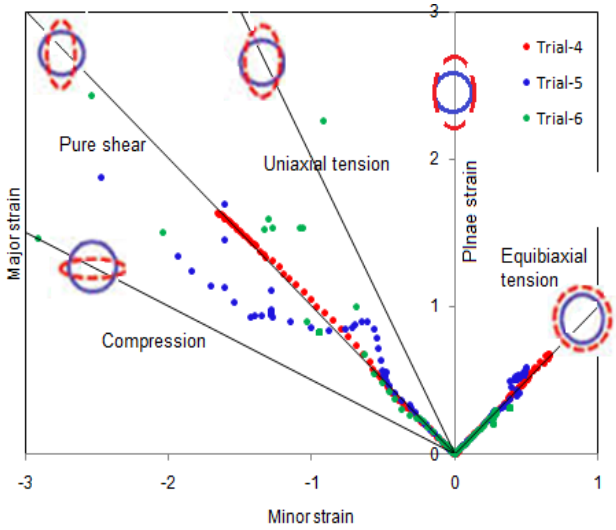

Figure 16: Forming limit diagram with damage in the cups of 1.0 mm blank thickness

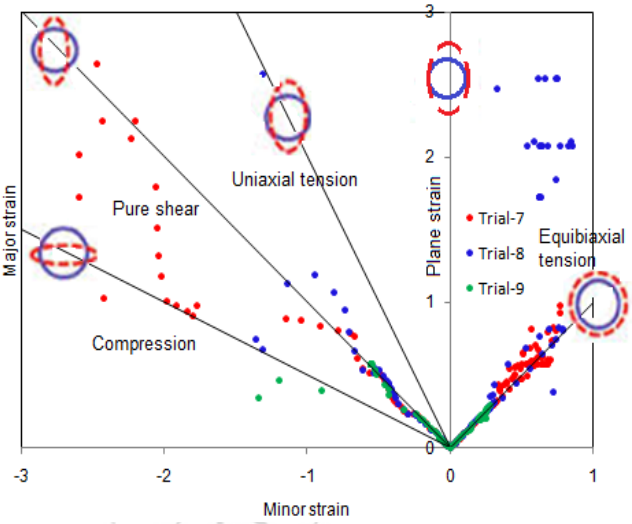

Figure 17: Forming limit diagram with damage in the cups of 1.2 mm blank thickness

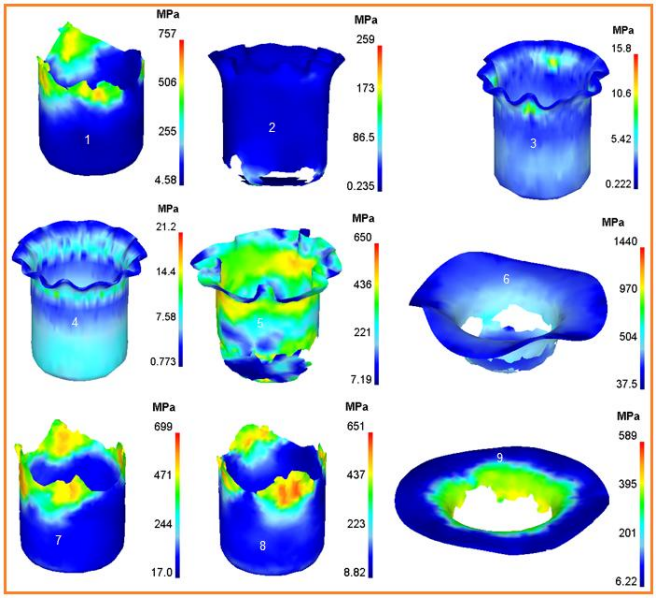

Figure 18: Shear strengths and damages of the cups.

Figure 19: Experimental validation of deep drawing nickel 201

5. Conclusions

In the present work, Nickel 201 was used to fabricate cylindrical cups. The investigation was focused on the process parameters such as punch velocity, coefficient of friction, displacement per step and strain rate. The major process parameters which could the influence the deep drawing capability of nickel 201 cylindrical cups, were punch velocity and strain rate. The effective stress was increased with an increase in the punch velocity. The equivalent stress was increased from 10–100 s–1 while at quasi-static strain conditions below strain rate of 10 s–1 the total elongation is smaller and the material rupture at lower equivalent strains.

6. Acknowledgment

The author wishes to thank University Grants Commission (UGC), New Delhi, India for financial assisting this project.

References

[1] A. C. Reddy, Evaluation of local thinning during cup drawing of gas cylinder steel using isotropic criteria, International Journal of Engineering and Materials Sciences, 5 (2), pp. 71-76, 2012.
[2] H. Zein, M. El-Sherbiny, M. Abd-Rabou, M. El Shazly, Effect of Die Design Parameters on Thinning of Sheet Metal in the Deep Drawing Process, American Journal of Mechanical Engineering, 1 (2), 20-29, 2013.
[3] A. C. Reddy, T. Kishen Kumar Reddy and M. Vidya Sagar, Experimental characterization of warm deep drawing process for EDD steel, International Journal of Multidisciplinary Research & Advances in Engineering, 4(3), pp.53-62, 2012.
[4] A. C. Reddy, Finite element analysis of reverse superplastic blow forming of Ti-Al-4V alloy for optimized control of thickness variation using ABAQUS, Journal of Manufacturing Engineering, 1(1), pp.06-09, 2006.
[5] A. C. Reddy, Homogenization and Parametric Consequence of Warm Deep Drawing Process for 1050A Aluminum Alloy: Validation through FEA, International Journal of Science and Research, 4(4), pp. 2034-2042, 2015.
[6] A. C. Reddy, Parametric Optimization of Warm Deep Drawing Process of 2014T6 Aluminum Alloy Using FEA, International Journal of Scientific & Engineering Research, 6(5), pp. 1016-1024, 2015.
[7] A. C. Reddy, Parametric Significance of Warm Drawing Process for 2024T4 Aluminum Alloy through FEA, International Journal of Science and Research, 4(5), pp. 2345-2351, 2015.
[8] A. C. Reddy, Formability of Warm Deep Drawing Process for AA1050-H18 Pyramidal Cups, International Journal of Science and Research, 4(7), pp. 2111-2119, 2015.
[9] A. C. Reddy, Formability of Warm Deep Drawing Process for AA1050-H18 Rectangular Cups, International Journal of Mechanical and Production Engineering Research and Development, 5(4), pp. 85-97, 2015.
[10] A. C. Reddy, Formability of superplastic deep drawing process with moving blank holder for AA1050-H18 conical cups, International Journal of Research in Engineering and Technology, 4(8), pp. 124-132, 2015.
[11] A. C. Reddy, Performance of Warm Deep Drawing Process for AA1050 Cylindrical Cups with and Without Blank Holding Force, International Journal of Scientific Research, 4(10), pp. 358-365, 2015.
[12] A. C. Reddy, Finite Element Analysis of Warm Deep Drawing Process for 2017T4 Aluminum Alloy: Parametric Significance Using Taguchi Technique, International Journal of Advanced Research, 3(5), pp. 1247-1255, 2015.
[13] A. C. Reddy, Formability of High Temperature and High Strain Rate Superplastic Deep Drawing Process for AA2219 Cylindrical Cups, International Journal of Advanced Research, 3(10), pp. 1016-1024, 2015.
[14] A. C. Reddy, High temperature and high strain rate superplastic deep drawing process for AA2618 alloy cylindrical cups, International Journal of Scientific Engineering and Applied Science, 2(2), pp. 35-41, 2016
[15] A. C. Reddy, Practicability of High Temperature and High Strain Rate Superplastic Deep Drawing Process for AA3003 Alloy Cylindrical Cups, International Journal of Engineering Inventions, 5(3), pp. 16-23, 2016
[16] A. C. Reddy, High temperature and high strain rate superplastic deep drawing process for AA5049 alloy cylindrical cups, International Journal of Engineering Sciences & Research Technology, 5(2), pp. 261-268, 2016.
[17] A. C. Reddy, Suitability of High Temperature and High Strain Rate Superplastic Deep Drawing Process for AA5052 Alloy, International Journal of Engineering and Advanced Research Technology, 2(3), pp. 11-14, 2016.
[18] Y.Q. Guo, Y.M. Li, F. Bogard, K. Debrey, An efficient pseudo-inverse approach for damage modelling in the sheet forming process, Journal of Materials Processing Technology, Vol. 151, pp. 88-97, 2004.
[19] F. J. Carignan, E. Rabinowicz, Friction and wear at high sliding speed. ASLE Transactions, 24(4), pp. 451–459, 1979.